INORGANIC CHEMISTRY
FRONTIERS

PAPER

2,2′-Bis(3-hydroxy-1,4-naphthoquinone)/CMK-3 nanocomposite as cathode material for lithium-ion batteries†

Cite this: DOI: 10.1039/c3qi00076a

Hao Li, Wenchao Duan, Qing Zhao, Fangyi Cheng, Jing Liang and Jun Chen*

Received 18th October 2013,
Accepted 18th November 2013

DOI: 10.1039/c3qi00076a

rsc.li/frontiers-inorganic

An inorganic–organic nanocomposite with the filling of 2,2′-bis(3-hydroxy-1,4-naphthoquinone) (H_2bhnq) in the pores of CMK-3 mesoporous carbon, which was synthesized by a simple impregnation method, was employed as a new cathode material for rechargeable lithium-ion batteries (LIBs). The characterization of the nanocomposite by wide-angle and low-angle X-ray diffraction, Brunauer–Emmett–Teller (BET), scanning electron microscopy (SEM) and transmission electron microscopy (TEM) showed the efficient loading of H_2bhnp within the nanosized pores of CMK-3 carbon. The nanocomposite delivered an initial discharge capacity of 308.6 mAh g^{-1} at 0.1 C rate and a capacity retention of 202.6 mAh g^{-1} after 50 cycles. The reversible capacities were 124.0 mAh g^{-1} at a higher rate of 10 C. The enhanced cycling stability and high-rate capability is attributed to the fact that neat H_2bhnq was distributed in the nanochannels of the conductive carbon framework CMK-3. This constrains the dissolution of the embedded H_2bhnq. The results imply that the nanoconfinement with the pores of inorganic materials such as CMK-3 to fill organic active materials is important to improve the electrochemical performance of lithium-ion batteries.

Introduction

Lithium-ion batteries (LIBs) are representative electrochemical energy storage and conversion devices to power portable electronics. For applications in the emerging fields of electric vehicles (EV) and smart grids, there is an increasing requirement of improved safety, lower cost and higher energy density.[1–3] Organic carbonyl compounds have attracted extensive attention as alternative active materials for LIBs due to their wide availability, environmentally-benign synthesis, high theoretical capacity and structural flexibility.[4–8] Unfortunately, the liable dissolution of small organic molecules in aprotic electrolyte and the intrinsically poor electrical conductivity of organic compounds usually lead to rapid capacity fading and a lower rate capability, severely hindering their practical application.

Several innovative strategies have been attempted to address the solubility problem of organic compounds in electrolytes, including increasing the molecular weight by polymerization,[9–14] fabricating coordination compounds through Li–O or Li–N bond bridges[15–18] and using a solid or quasi-solid-state electrolyte to replace the traditional liquid electrolyte.[19,20] On the other hand, two common approaches have been used to enhance the electrical conductivity of organic electrodes. One is the incorporation of heteroaromatic structures in organic molecular frameworks[21] while the other is resorting the active materials to conductive additives such as carbon nanostructures.[22–25] Recently, a composite of 9,10-anthraquinone (AQ) and mesoporous carbon has been proposed to simultaneously overcome the dissolution and poor conductivity issue of AQ,[26] resulting in an improved cycle life and rate performance. Nevertheless, the relatively large open porous structure (with pore diameter of 50–60 nm) of the employed carbon cannot effectively prevent the dissolution of AQ in the electrolyte and thus only a limited capacity of 97 mAh g^{-1} has been maintained after 50 cycles for the composite electrode. An appropriate mesoporous carbon matrix with a smaller pore diameter for better confining organic material is desirable to attain an enhanced electrode performance.

Mesoporous CMK-3 carbon has been extensively investigated for potential applications such as catalyst support, hydrogen storage, supercapacitors and Li-S batteries,[27–29] owning to its well-ordered porous structure, uniform small

Key Laboratory of Advanced Energy Materials Chemistry (Ministry of Education), College of Chemistry, Collaborative Innovation Center of Chemical Science and Engineering, Nankai University, Tianjin 300071, P. R. China.
E-mail: chenabc@nankai.edu; Fax: +86-22-23509571; Tel: +86-22-23506808

† Electronic supplementary information (ESI) available: the synthetic route of H_2bhnq, the FT-IR spectrum, ^{1}H and ^{13}C spectra, TG-DSC curves and SEM images. See DOI: 10.1039/c3qi00076a

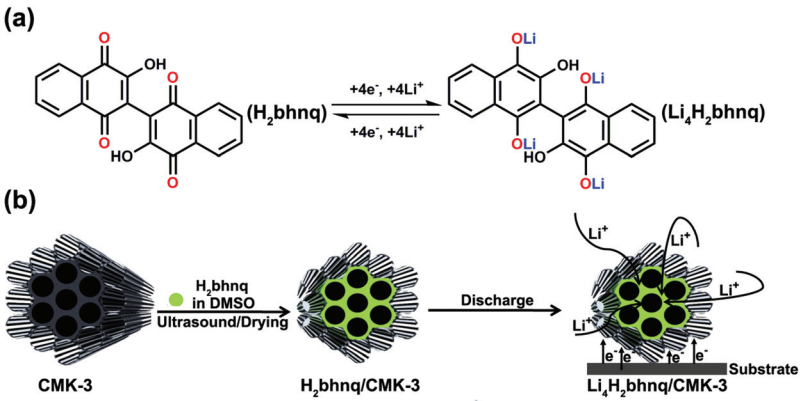

Scheme 1 A schematic illustration for (a) the proposed electrochemical redox mechanism of H_2bhnq and (b) the preparation and electrode reaction of the H_2bhnq/CMK-3 nanocomposite.

pore size (6–7 nm), large specific surface area and high conductivity.[30] These properties of CMK-3 should make it a suitable matrix for loading soluble organic electrode materials. In this work, we apply CMK-3 to confine 2,2′-bis(3-hydroxy-1,4-naphthoquinone) (H_2bhnq). As a flexible hinge like ligand, H_2bhnq has been widely used in coordination chemistry to construct metal–organic frameworks.[31,32] However, to the best of our knowledge, it has not been reported for use in LIBs. Theoretically, H_2bhnq could react with four Li per molecule, giving a high specific capacity of 309.6 mAh g^{-1} (Scheme 1a). Herein, we encapsulate H_2bhnq in CMK-3 by a simple room-temperature impregnation method and demonstrate that the as-synthesized nanocomposite exhibits a respectable lithium-storage performance (Scheme 1b). It is found that the hurdles of poor conductivity and easy dissolution of H_2bhnq in the aprotic electrolyte can be largely surmounted owing to the restriction of the nanoporous structure and the high electrical conductivity of the carbon framework.

Experimental

Synthesis

All reagents are of analytic grade unless stated. H_2bhnq was synthesized by an oxidization method (Scheme S1, ESI†).[33] In a typical synthesis, 1 mmol bi-1,4-naphthoquinone was dissolved in 5 mL 1,4-dioxane and an 0.75 mL aqueous NaOH solution (5 mol L^{-1}). Five drops of aqueous H_2O_2 (30%) were then added to the obtained suspension, forming a clear red solution. The mixture was vigorously stirred for 5 min and the insoluble reagent was filtered off. After the evaporation of the filtrate, the residue was recrystallized from glacial acetic acid to generate yellow amorphous powders (0.242 g, 70% yield).

The H_2bhnq/CMK-3 nanocomposite was prepared by a simple impregnation method. H_2bhnq (50 mg) was first dissolved in 1 mL dimethyl sulfoxide (DMSO) and 50 mg CMK-3 (purchased from Nanjing JiCang) was then added to the solution. The mixture was ultrasonically treated for 30 min. After that, the solvent was removed under vacuum to obtain the H_2bhnq/CMK-3 nanocomposite. Samples with different compositions were also prepared by altering the mass ratio of H_2bhnq and CMK-3.

Material characterization

The structures of H_2bhnq were determined by ^{1}H and ^{13}C nuclear magnetic resonance spectroscopy (NMR, Varian Mercury Vx300 MHz spectrometer) and elemental analysis (German, VarioEL). The IR spectra were collected at room temperature using a FTIR-650 spectrometer (Tianjin Gangdong) between 4000 and 400 cm^{-1}. The TG measurements were performed under an Ar atmosphere with a NETZSCH TG 209 using a heating rate of 5 °C min^{-1}. The obtained H_2bhnq/CMK-3 composites were characterized by powder X-ray diffraction in the wide 2θ range of 10–80° (Rigaku MiniFlex600, CuKα radiation) and in the small 2θ range of 0.6–6° (Bruker D8FOCUS, CuKα radiation). The morphologies and microstructures of the materials were observed using scanning electron microscopy (SEM, JEOL JSM7500F) and transmission electron microscopy (TEM, Philips Tecnai-F20). The surface area and pore size distribution were measured by N_2 adsorption–desorption isotherms at 77 K on a BELSORP-mini instrument.

Electrochemical investigation

CR2032 coin-type cells with a lithium plate anode were assembled in a glovebox filled with argon. The composite electrodes were made by blending 80 wt% H_2bhnq/CMK-3 (mass ratio = 1 : 1) with 10 wt% of carbon black (Vulcan XC72, Cabot) and 10 wt% of polyvinylidenedifluoride (PVDF) as a binder. The comparative H_2bhnq electrodes were composed of 40 wt% H_2bhnq, 50 wt% carbon black and 10 wt% PVDF. The electrolyte contained 1 M $LiFP_6$ in ethylene carbonate–dimethyl carbonate (EC–DMC, volume ratio 1 : 1). The charge–discharge experiments were carried out on a Land CT2001A cell testing system within the potential range of 1.8–3.3 V using different current rates. The capacities were calculated by only considering the active mass of the working electrodes as the carbon additive contributed negligibly to the overall capacity. Impedance measurements were conducted using a 2273

potentiostat/galvanostat workstation with an amplitude of 5 mV over the frequency range from 100 kHz to 100 mHz. All of the electrochemical tests were performed at room temperature.

Results and discussion

Material characterization

The elemental analysis, IR, ^{1}H and ^{13}C NMR spectra (Fig. S1, S2 ESI†) of the obtained sample clearly indicate the successful synthesis of the target H_2bhnq. From the result of the thermogravimetric analysis (Fig. S3, ESI†), H_2bhnq exhibits a considerable thermal stability up to around 260 °C, which is an advantageous factor concerning the safety of organic electrode materials. The H_2bhnq/CMK-3 nanocomposites were prepared by a simple impregnation method using a DMSO solvent. The interconnected mesoporous framework and high thermal stability of CMK-3 as well as the excellent solubility of H_2bhnq in DMSO allow for both the high dispersion and high loading of H_2bhnq.[27,29,30] Fig. 1 shows the wide-angle and low-angle XRD patterns of H_2bhnq, CMK-3 and the H_2bhnq/CMK-3 nanocomposite with a varied content of H_2bhnq. As shown in Fig. 1a, no sharp diffraction peaks of H_2bhnq can be observed when the weight ratio of H_2bhnq was lower than 50%, which indicates that H_2bhnq is highly dispersed in the pores of CMK-3 at the nanoscale.[26,29] Such a highly dispersed amorphous state could improve the electrical conductivity of the composite. On further increasing the H_2bhnq content, the peaks of H_2bhnq gradually emerge, demonstrating the mixed state of the amorphous and crystalline structures in the composite.[26,34] The low-angle XRD patterns in the 2θ range of 0.6–6° (Fig. 1b) display a similar trend. The sharp peak assigned to CMK-3 at 1.3° gradually declines as the content of H_2bhnq is increased and disappears when the amount of H_2bhnq is higher than 50 wt%, further proving the filling of the channels with H_2bhnq.

The specific surface areas of CMK-3 and a representative H_2bhnq/CMK-3 (mass ratio = 1 : 1) composite were characterized by N_2 adsorption–desorption isotherms (Fig. 2a) and the corresponding pore size distribution (PSD, Fig. 2b) was determined using the BJH method. After the impregnation of H_2bhnq, the BET surface area decreases from 1084.5 to 54.9 $m^2\ g^{-1}$, while the mesoporous volume drops from 1.09 to 0.20 $cm^3\ g^{-1}$. These results provide further evidence to support the fact that the H_2bhnq molecules were accommodated in the mesopores of CMK-3.[34]

The morphology change of CMK-3 before and after impregnation is investigated using SEM. CMK-3 materials have an extremely high surface area and a highly ordered porous structure, which give them the appearance of nanochanneled

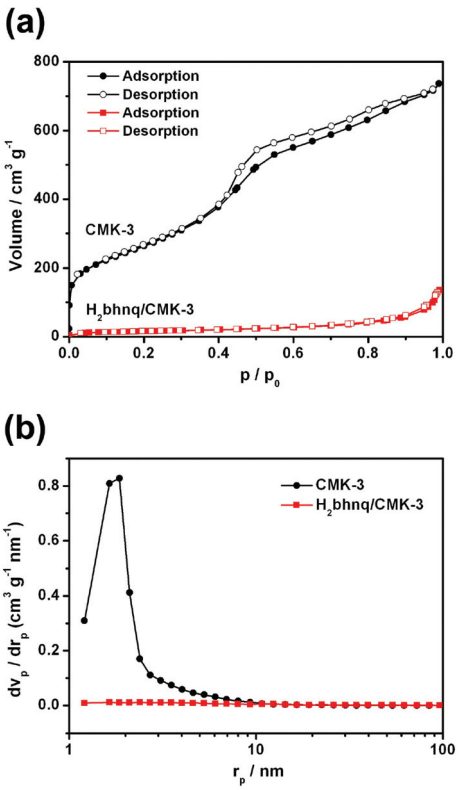

Fig. 2 (a) The nitrogen adsorption–desorption isotherms and (b) the corresponding pore-size distributions of CMK-3 and H_2bhnq/CMK-3 (mass ratio = 1 : 1).

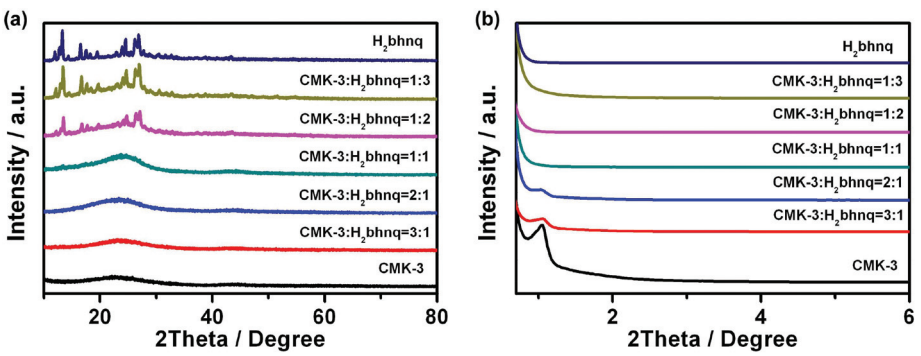

Fig. 1 (a) The wide-angle and (b) low-angle XRD patterns of CMK-3, H_2bhnp, and the H_2bhnq/CMK-3 composites with different amounts of H_2bhnq.

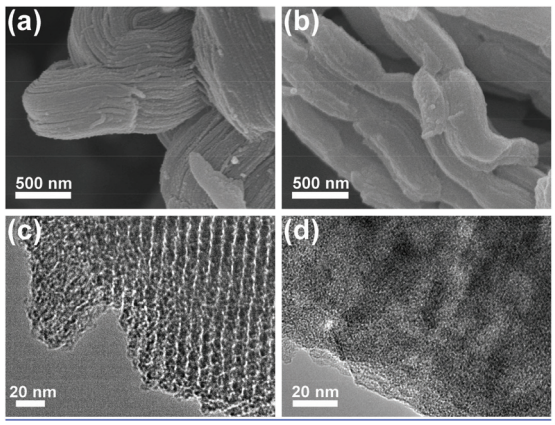

Fig. 3 SEM images (a,b) and TEM images (c,d) of CMK-3 (a,c) and H_2bhnq/CMK-3 with 50 wt% H_2bhnq (b,d).

carbon scaffolds (Fig. 3a).[28,30] However, after impregnation of 50 wt% H_2bhnq, the surface of CMK-3 turns smooth (Fig. 3b), indicating the filling of H_2bhnq in the nanochannels of CMK-3. Moreover, when the content of H_2bhnq reached higher than 50 wt%, the excess bulk H_2bhnq was presented in the form of crystals, as can be clearly seen in the SEM image (Fig. S4, ESI†). This indicates that the channel of CMK-3 was fully filled, which is in conformity with the wide-angle XRD results. The filling of the carbon channels with H_2bhnq was further verified by a TEM image. Uniform channels with a diameter of 6–7 nm are evident in the TEM image of pure CMK-3 (Fig. 3c) but largely vanish after impregnation (Fig. 3d). More importantly, no bulk H_2bhnq particles were observed on the external surface, which suggests that the incorporation of H_2bhnq is restricted to the inner pores of CMK-3.[34]

Based on the above results, the H_2bhnq molecules were successfully anchored into the pore channels of CMK-3 ordered mesoporous carbon through the facile impregnation method. When the mass ratio of H_2bhnq reaches 50%, the pores are almost fully filled. The density of H_2bhnq is 1.50 g cm^{-3}. The pore volume of CMK-3 is 1.09 cm^3 g^{-1}, according to the BET test. It is noted that a maximum of 1.63 g ($m_s = v_p \times \rho_{H_2bhnq}$) of H_2bhnq can be impregnated into the pores of 1.00 g of CMK-3. The weight ratio of H_2bhnq was adjusted to be less than 62% to provide a transport pathway for the Li^+ ions and to allow for the expansion of the pore content on full lithiation to Li_4H_2bhnq. Thus, the synthesized H_2bhnq/CMK-3 composite with 50 wt% H_2bhnq (denoted as H_2bhnq/CMK-3 hereafter) was selected as a cathode material for the electrochemical test.

Electrochemical performance

Fig. 4a–b shows the charge and discharge curves of the neat H_2bhnq and the H_2bhnq/CMK-3 composite. Different capacity–voltage profiles can be observed. For H_2bhnq, the discharge curve has a flat voltage plateau at about 2.95 V, which is followed by relatively slopping plateaus. The average charge and discharge voltages are 2.53 and 2.36 V, respectively. The H_2bhnq/CMK-3 composite electrode exhibits slopping charge–discharge curves without an apparent plateaus and with average charge–discharge voltages of 2.48/2.30 V. This feature of the charge–discharge curves suggests the prominent nanosize effect[35,36] on the electrochemical behaviour of H_2bhnq that is confined in the nanosized channel of the carbon scaffold. The initial discharge capacities of H_2bhnq and the nanocomposite are 285.6 and 308.6 mAh g^{-1}, respectively. The latter capacity is extremely close to the theoretical value of 309.6 mAh g^{-1}, demonstrating that the use of the CMK-3 scaffold enables the full utilization of H_2bhnq, of which each carbonyl functional group reacts with one lithium to form a lithium enolate (Scheme 1). Meanwhile, H_2bhnq displays a high-specific energy of 715 W h kg^{-1} (based on the mass of active materials), which is compared favourably to other organic carbonyl compounds.[24]

The cycling performance of the electrodes made with H_2bhnq and H_2bhnq/CMK-3 is measured at 0.1 C rate. As shown in Fig. 4c, the capacity of H_2bhnq decreases rapidly after the first cycle. After 50 cycles, the discharge capacity only remains at 75.2 mAh g^{-1}, corresponding to a capacity fading of 73.7%. The poor cycling stability is ascribed to the dissolution of H_2bhnq into the electrolyte,[11] which is confirmed by the fact that the electrolyte turns red after charge–discharge testing. However, a much better stability upon cycling has been observed for H_2bhnq/CMK-3. After 50 cycles, a much higher capacity of 202.6 mAh g^{-1} is maintained. Meanwhile, the initial charge–discharge Coulombic efficiency of the composite is 85.9%, which is higher than that of H_2bhnq (81.5%). After several cycles, the Coulombic efficiency can reach higher than 99%. All the results illustrate that the encapsulation of H_2bhnq into CMK-3 could effectively inhibit the dissolution of H_2bhnq and thus improves its cycle stability.

The rate performance of H_2bhnq and H_2bhnq/CMK-3 was also tested (Fig. 4d). Compared to neat H_2bhnq, the composite sample exhibited a much better rate capability. The discharge capacities at 0.5 C are 154.3 and 245.8 mAh g^{-1} for H_2bhnq and H_2bhnq/CMK-3, respectively. At a high rate of 10 C, for which the electronic conductivity of the electrode materials is crucial,[21–24] the discharge capacity of the nanocomposite is approximately 4 times higher than that of H_2bhnq. The improved rate performance of the composite derives from the high conductivity and the ordered porous channels of CMK-3, which ensure the facile electron and ion transport.[37]

To further understand the role of CMK-3 in the composite, the structure of the electrode materials after the charge–discharge cycles was characterized by SEM and TEM. The SEM images (Fig. S5, ESI†) show that the morphology of CMK-3 was essentially preserved after the charge–discharge progress, suggesting the high structural stability of CMK-3. This could guarantee the integrity of the composite electrode during the electrochemical test. The TEM image of the nanocomposite after 50 cycles also shows a rodlike morphology (Fig. 5), which is in good agreement with the SEM result. It should be noted that no porous channel structure can be observed on the composite sample, implying that H_2bhnq is well confined within the pores of CMK-3 during the whole charge–discharge

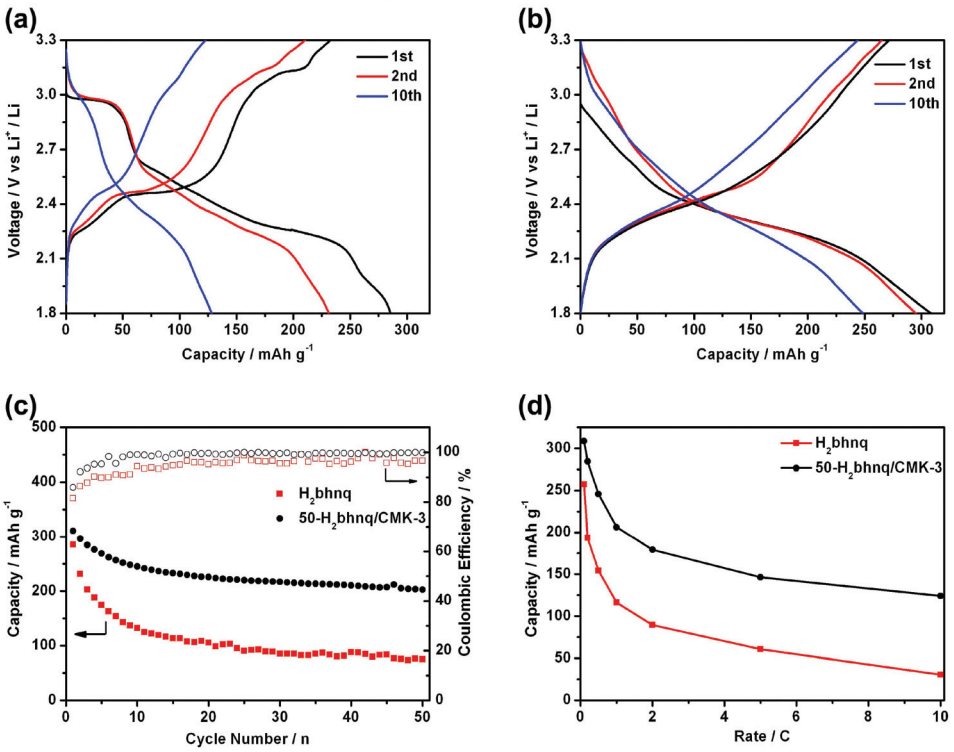

Fig. 4 The electrochemical characterization of H_2bhnq and H_2bhnq/CMK-3: (a) the discharge–charge curves of H_2bhnq at 0.1 C rate, (b) the discharge–charge curves of H_2bhnq/CMK-3 at 0.1 C rate, (c) the cycling performance and the corresponding Coulombic efficiency at a rate of 0.1 C and (d) the rate capability.

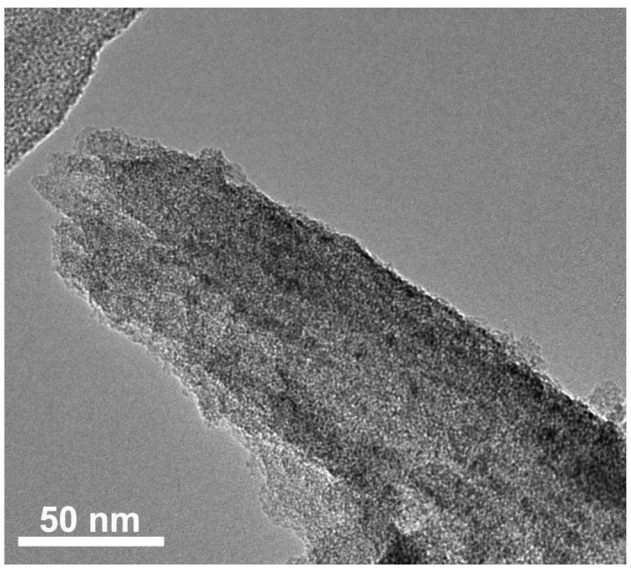

Fig. 5 A TEM image of H_2bhnq/CMK-3 after 50 charge–discharge cycles.

process, consequently prolonging the cycle life of the composite electrode.

In order to analyze the difference of the rate properties between H_2bhnq and H_2bhnq/CMK-3, the impedance spectra of the two electrodes after different cycles were collected (Fig. 6). All of the profiles show a semicircle in the high-

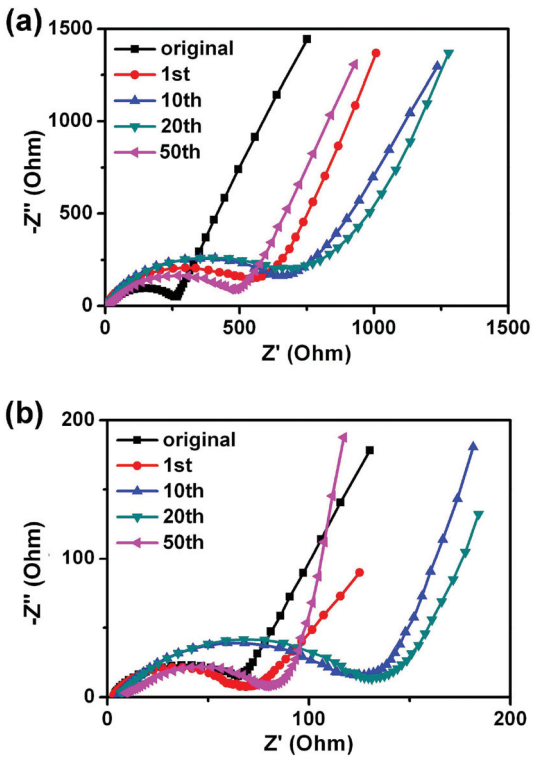

Fig. 6 The EIS of H_2bhnq (a) and H_2bhnq/CMK-3 (b) tested at the potential of 2.3 V and at cycling rate of 0.1 C.

frequency regions and an inclined line in the low-frequency region. The semicircle can be assigned to the combination of the charge-transfer resistances at the electrode surface and the double-layer capacitance between the electrolyte and the cathode.[38,39] The impedances increase with the cycle number for the first several cycles and then decrease for both samples. This phenomenon is relevant to the dissolution of active materials and agrees well with the previous report.[26] It is worth noting that the charge transfer resistance of H_2bhnq is much higher than that of the nanocomposite at the same cycle, indicating that the conductivity can be greatly enhanced after the uniform dispersion of H_2bhnq in the CMK-3 nanopores owing to the high conductivity of the carbon framework.[40]

Therefore, the use of CMK-3 is effective to enhance the electrode performance of H_2bhnq, which is attributed to the following aspects. Firstly, the high dispersion of H_2bhnq in the channels of CMK-3 reduces the dimension of the H_2bhnq into the nanoscale and thus provides more active sites for the electrode reactions, enabling the full utilization of the active mass. Secondly, the small channels of CMK-3 greatly restrict the dissolution of the well enwrapped H_2bhnq, ensuring the long cycle life of the composite electrode. Thirdly, CMK-3 acts as a substrate offering a sufficient percolation network for electrons and the nanosized H_2bhnq shortens the Li-ion transport distance, resulting in a high rate performance. These unique beneficial factors make H_2bhnq/CMK-3 a promising nanocomposite to enhance the electrochemical performance. It is noted that the carbon content of 50 wt% is slightly higher than the active materials and this could limit the overall capacity of the electrode. A further optimization of the electrode composition to increase the overall capacity of the electrode is in the study.

Conclusions

A facile impregnation method was employed to incorporate the H_2bhnq molecules into the pore channels of ordered mesoporous CMK-3. Different instrumental analyses have demonstrated the successful loading of H_2bhnq within the pores of CMK-3. The H_2bhnq/CMK-3 nanocomposite with 50 wt% H_2bhnq can provide a discharge capacity of 308.6 mAh g^{-1} at 0.1 C in the first cycle. The capacity was kept at 202.6 mAh g^{-1} after 50 cycles. At a high rate of 10 C, reversible capacities of 124.0 mAh g^{-1} are obtained. The results suggest that confining organic electrode materials in inorganic CMK-3 could not only improve the conductivity, but also protect them from dissolving into the electrolyte. This work should enlighten the application of inorganic–organic nanocomposites such as organic carbonyl materials in CMK-3 for advanced lithium-ion batteries.

Acknowledgements

This work was supported by the Programs of National 973 (2011CB935900), NSFC (21231005), 111 Project (B12015), and Tianjin High-Tech (13JCQNJC06400).

Notes and references

1 M. Armand and J. M. Tarascon, *Nature*, 2008, **451**, 652.
2 J. Chen and F. Cheng, *Acc. Chem. Res.*, 2009, **42**, 713.
3 F. Cheng, J. Liang, Z. Tao and J. Chen, *Adv. Mater.*, 2011, **23**, 1695.
4 H. Chen, M. Armand, M. Courty, M. Jiang, C. P. Grey, F. Dolhem, J. M. Tarascon and P. Poizot, *J. Am. Chem. Soc.*, 2009, **131**, 8984.
5 M. Armand, S. Grugeon, H. Vezin, S. Laruelle, P. Ribière, P. Poizot and J. M. Tarascon, *Nat. Mater.*, 2009, **8**, 120.
6 Y. Liang, Z. Tao and J. Chen, *Adv. Energy Mater.*, 2012, **2**, 742.
7 P. Poizot and F. Dolhem, *Energy Environ. Sci.*, 2011, **4**, 2003.
8 W. Choi, D. Harada, K. Oyaizu and H. Nishide, *J. Am. Chem. Soc.*, 2011, **133**, 19839.
9 D. Häringer, *J. Electrochem. Soc.*, 1999, **146**, 2393.
10 X. Han, C. Chang, L. Yuan, T. Sun and J. Sun, *Adv. Mater.*, 2007, **19**, 1616.
11 Z. Song, H. Zhan and Y. Zhou, *Chem. Commun.*, 2009, 448.
12 K. Liu, J. Zheng, G. Zhong and Y. Yang, *J. Mater. Chem.*, 2011, **21**, 4125.
13 T. Nokami, T. Matsuo, Y. Inatomi, N. Hojo, T. Tsukagoshi, H. Yoshizawa, A. Shimizu, H. Kuramoto, K. Komae, H. Tsuyama and J. Yoshida, *J. Am. Chem. Soc.*, 2012, **134**, 19694.
14 T. Le Gall, K. H. Reiman, M. C. Grossel and J. R. Owen, *J. Power Sources*, 2003, **119–121**, 316.
15 J. Xiang, C. Chang, M. Li, S. Wu, L. Yuan and J. Sun, *Cryst. Growth Des.*, 2008, **8**, 280.
16 S. Renault, J. Geng, F. Dolhem and P. Poizot, *Chem. Commun.*, 2011, **47**, 2414.
17 R. Zeng, X. Li, Y. Qiu, W. Li, J. Yi, D. Lu, C. Tan and M. Xu, *Electrochem. Commun.*, 2010, **12**, 1253.
18 S. Wang, L. Wang, K. Zhang, Z. Zhu, Z. Tao and J. Chen, *Nano Lett.*, 2013, **13**, 4404.
19 Y. Hanyu and I. Honma, *Sci. Rep.*, 2012, **2**, 453.
20 W. Huang, Z. Zhu, L. Wang, S. Wang, H. Li, Z. Tao, J. Shi, L. Guan and J. Chen, *Angew. Chem., Int. Ed.*, 2013, **52**, 9162.
21 Y. Liang, P. Zhang, S. Yang, Z. Tao and J. Chen, *Adv. Energy Mater.*, 2013, **3**, 600.
22 W. Guo, Y. Yin, S. Xin, Y. Guo and L. Wan, *Energy Environ. Sci.*, 2012, **5**, 5221.
23 Z. Song, T. Xu, M. L. Gordin, Y. B. Jiang, I. T. Bae, Q. Xiao, H. Zhan, J. Liu and D. Wang, *Nano Lett.*, 2012, **12**, 2205.
24 Y. Liang, P. Zhang and J. Chen, *Chem. Sci.*, 2013, **4**, 1330.
25 S. Renault, D. Brandell, T. Gustafsson and K. Edström, *Chem. Commun.*, 2013, **49**, 1945.
26 L. Zhao, W. Wang, A. Wang, Z. Yu, S. Chen and Y. Yang, *J. Electrochem. Soc.*, 2011, **158**, A991.
27 Y. Zhai, Y. Dou, D. Zhao, P. F. Fulvio, R. T. Mayes and S. Dai, *Adv. Mater.*, 2011, **23**, 4828.
28 A. Gutowska, L. Li, Y. Shin, C. M. Wang, X. S. Li, J. C. Linehan, R. S. Smith, B. D. Kay, B. Schmid, W. Shaw, M. Gutowski and T. Autrey, *Angew. Chem., Int. Ed.*, 2005, **44**, 3578.

29 X. Ji, K. T. Lee and L. F. Nazar, *Nat. Mater.*, 2009, **8**, 500.
30 S. Jun, S. H. Joo, R. Ryoo, M. Kruk, M. Jaroniec, Z. Liu, T. Ohsuna and O. Terasaki, *J. Am. Chem. Soc.*, 2000, **122**, 10712.
31 K. Yamada, H. Tanaka, S. Yagishita, K. Adachi, T. Uemura, S. Kitagawa and S. Kawata, *Inorg. Chem.*, 2006, **45**, 4322.
32 F. L. S. Bustamante, J. M. Metello, F. A. V. de Castro, C. B. Pinheiro, M. D. Pereira and M. Lanznaster, *Inorg. Chem.*, 2013, **52**, 1167.
33 H. Laatsch, *Liebigs Ann. Chem.*, 1983, **1983**, 1886.
34 S. Zhu, H. Zhou, M. Hibino, I. Honma and M. Ichihara, *Adv. Funct. Mater.*, 2005, **15**, 381.
35 M. Okubo, E. Hosono, J. Kim, M. Enomoto, N. Kojima, T. Kudo, H. Zhou and I. Honma, *J. Am. Chem. Soc.*, 2007, **129**, 7444.
36 M. Okubo, J. Kim, T. Kudo, H. Zhou and I. Honma, *J. Phys. Chem. C*, 2009, **113**, 15337.
37 K. Zhang, Z. Hu and J. Chen, *J. Energy Chem.*, 2013, **22**, 214.
38 F. Cheng, H. Wang, Z. Zhu, Y. Wang, T. Zhang, Z. Tao and J. Chen, *Energy Environ. Sci.*, 2011, **4**, 3668.
39 Z. Zhu, F. Cheng and J. Chen, *J. Mater. Chem. A*, 2013, **1**, 9484.
40 J. Fan, T. Wang, C. Yu, B. Tu, Z. Jiang and D. Zhao, *Adv. Mater.*, 2004, **16**, 1432.